Journal of the Nigerian Association of Mathematical Physics
Volume 12 (May, 2008), 225 – 236
© *J. of NAMP*

Pressure gradient and pressure derivative characteristics of a horizontal well subject to bottom water drive mechanism

E. S. Adewole
Department of Petroleum Engineering,
University of Benin, Benin City, Nigeria.
e-mail: steveadewole@yahoo.co.uk Phone: 08039237561

Abstract

Two kinds of dimensionless pressure derivatives, $\partial p_D / \partial t_D$ ***and*** $t_D \partial p_D / \partial t_D$ ***, have been studied for a horizontal well in a bounded reservoir subject to bottom water drive mechanism. The influence of dimensionless well length and reservoir geometry was investigated. Possible flow periods for a given well completion were identified. Results show that dimensionless well length is a major determinant of the magnitude of both derivatives, especially at early flow times, and determines the number of flow periods obtainable. Well length modification can be used to produce the effects of a square reservoir with a rectangular reservoir and vice versa. Finally, large reservoirs are found to produce more clean oil than small reservoirs, given the same well completion and reservoir properties.***

1.0 Introduction

In a bottom water drive reservoir, water encroaches into the wellbore directly from the bottom of the well, leading to water breakthrough. This can cause prolonged well shut down and expensive workover job on the wellbore.

Dimensionless pressure derivatives of the type $t_D \partial p_D / \partial t_D$ were first introduced into the petroleum literature by Bourdet et al [12]. Dimensionless pressure derivative plots most commonly used for diagnosis today and for which soft wares are available to generate, have the forms $t_D \partial p_D / \partial t_D$ or $\partial p_D / \partial \ln t_D$ and $\partial p_{wD} / 2\partial p_{wD} / \partial \ln t_D$. They expose both the wellbore and reservoir character more explicitly than the conventional test analysis techniques that were hitherto used in transient well test analysis. These derivatives are plotted on log-log axes against dimensionless time. Some of the plots show, depending on the nature of the plots, wellbore completion performance, damage index, presence or absence of boundaries, reservoir anisotropy, wellbore storage and skin factor.

When these commercial softwares produce dimensionless derivatives plots, interpretation may be difficult if an understanding of the behaviour of the physical reservoir system is lacking. This paper is therefore aimed at studying the possible trends and characteristics most likely to be observed on derivative plots if the horizontal well is subject to bottom water drive mechanism. In particular, factors affecting clean oil production in both square and rectangular oil field patterns are investigated. Both wellbore and skin are however not considered, not because they are not important or impossible to do so but an ideal behaviour is assumed.

Ozkan [3] studied a similar reservoir model but did not include the influence of field patterns on clean oil production and only laterally infinite reservoir pattern was discussed. This paper discusses the influence of reservoir geometry and assumes that all the external boundaries, except the bottom of the reservoir, are sealed. The study will therefore provide a wide range of flexible options for well completion than can guarantee clean oil production.

Nomenclature

$p_D = \frac{kh\Delta p}{141.2q\mu B}$; $t_D = \frac{0.001056kt}{\mu\phi c_t L^2}$; $i_D = \frac{2i}{L}\sqrt{\frac{k}{k_i}}$

i = positions along x or y or z axes, *ft*; $h_D = 1/L_D$; Δ = drop; p = pressure, psi;

k = permeability, *md*; h = pay thickness, *ft*; t = time, hours; q = flow rate, *STB/Day*;

μ = oil viscosity, *cp; B* = oil formation volume factor, *bbl/STB*;

c_t = total fluid compressibility, 1/*psi*; L = well length, *ft*;

erf = error function; τ = dimensionless dummy time variable;

DPG = dimensionless pressure gradient p'_D;

PDD = dimensionless pressure derivative, $t_D\, p'_D$

Subscripts

x, y, z = x, y, or z, directions;

D = dimensionless;

w = wellbore; *e* = external;

2.0 The basis of pressure derivatives

If
$$p_D = \int_0^{t_D} A(\tau)\bullet B(\tau)\bullet C(\tau)d\tau + \int_{t_{D1}}^{t_{D2}} D(\tau)\bullet E(\tau)\bullet F(\tau)d\tau. \tag{2.1}$$

then
$$\frac{\partial p_D}{\partial t} = A(t_D)\bullet B(t_D)\bullet C(t_D) + D(t_D) + E(t_D) + F(t_D). \tag{2.2}$$

and
$$t_D\frac{\partial p_D}{\partial t} = t_D A(t_D)\bullet B(t_D)\bullet C(t_D) + D(t_D) + E(t_D) + F(t_D) \tag{2.3}$$

Derivatives of the type in equation (2.2) were used in Refs. [4] to [6] in pressure transient test analysis. Dimensionless pressure gradients of the form in equation (2.2) can be used to delineate flow periods normally encountered in horizontal wells. This procedure eliminates guessing and the use of rigid approximation expressions. Changes in gradients would correspond to changes in flow periods and could therefore be used to easily estimate the integration intervals in equations of the type similar to equation (2.1).

3.0 Reservoir and mathematical description

An anisotropic reservoir with closed lateral boundaries is assumed. The reservoir contains a horizontal well and the reservoir energy for oil production is obtained from contiguous bottom water as shown in Figure 3.1. Origin of well axes is at center of the well; that is, at (x_D , y_D , z_D, L_D) = (0 , 0 , z_{wD}, $L_D/2$).

Accordingly, the dimensionless pressure distribution expression for this reservoir model is written as follows using Green's and source functions [3, 7, 8]:

$$p_D = \frac{4\pi}{y_{eD}x_{eD}} \int_0^{t_D} \left[1 + \frac{2x_{eD}}{\pi} \sum_{n=1}^{\infty} \frac{1}{n} \exp(-\frac{n^2\pi^2\tau}{x_{eD}^2}) \sin\frac{n\pi}{x_{eD}} \cos\frac{n\pi x_{wD}}{x_{eD}} \cos\frac{n\pi x_D}{x_{eD}}) \right] \bullet$$

$$\left[1 + 2\sum_{m=1}^{\infty} \exp(-\frac{m^2\pi^2\tau}{y_{eD}^2}) \cos\frac{m\pi y_{wD}}{y_{eD}} \cos\frac{m\pi y_D}{y_{eD}}) \right] \bullet \sum_{l=1}^{\infty} \exp(-\frac{(2l-1)^2\pi^2\tau}{4h_D^2}) \qquad (3.1)$$

$$\times \sin\frac{(2l-1)\pi z_{wD}}{2h_D} \sin\frac{(2l-1)\pi z_D}{2h_D}\, d\tau$$

Equation (3.1) shows all the possible reservoir boundaries that can be felt by pressure transients created in the horizontal well. However, not all of these boundaries can be felt in the same transient test period.

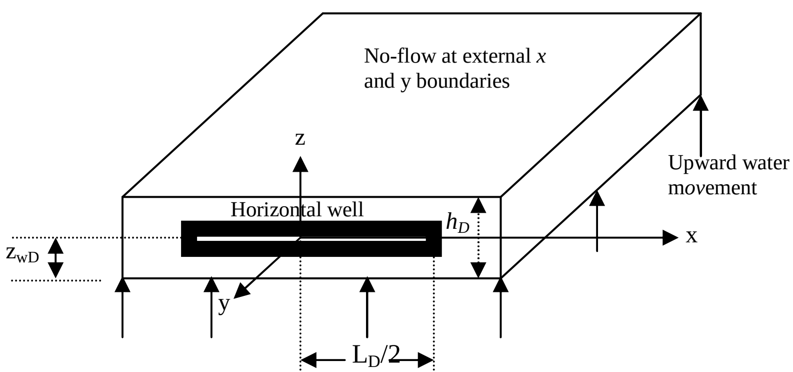

Figure 3.1: Bottom water drive reservoir model

The number of boundaries that can be felt in the event of a well test depends on

(1) reservoir anisotropy,
(2) production/injection rate,
(3) reservoir size, and
(4) the horizontal well length. Possible flow periods, i.e., boundaries that may be felt, and their pressure distributions are discussed below.

4.0 Solutions to equation (2.1)

Using the superposition theorem, if uniform rate prevails, the dimensionless pressure drop at the expiry of infinite-acting radial flow period and the commencement of effect of any boundary (wellbore or reservoir), the solution to equation (2.1) may be written as:

$$p_D = \frac{kk\alpha}{8k_y k_z L_D}\int_0^{t_D}\frac{e^{-\left[(y_D-y_{wD})^2+(z_D-z_{wD})^2\right]/4\tau}}{\tau}d\tau + \frac{4\pi}{y_{eD}x_{eD}}$$
$$\times\int_{t_{De}}^{t_D}\left[1+\frac{2x_{eD}}{\pi}\sum_{n=1}^{\infty}\frac{1}{n}\exp(-\frac{n^2\pi^2\tau}{x_{eD}^2}\sin\frac{n\pi}{x_{eD}}\cos\frac{n\pi x_{wD}}{x_{eD}}\cos\frac{n\pi x_D}{x_{eD}})\right] \tag{4.1}$$
$$\bullet\left[1+2\sum_{m=1}^{\infty}\exp(-\frac{m^2\pi^2\tau}{y_{eD}^2})\cos\frac{m\pi y_{wD}}{y_{eD}}\cos\frac{m\pi y_D}{y_{eD}})\right]$$
$$\bullet\sum_{l=1}^{\infty}\exp(-\frac{(2l-1)^2\pi^2\tau}{4h_D^2})\sin\frac{(2l-1)\pi z_{wD}}{2h_D}\sin\frac{(2l-1)\pi z_D}{2h_D}d\tau.$$

4.1 Early radial flow period

This is the first noticeable flow period at inception of transient flow in the well and is unaffected by reservoir or wellbore boundaries. During this period, flow gradients portray the reservoir as infinite. This period is terminated immediately a boundary of any kind is felt. The dimensionless pressure distribution during this period is

$$p_D = \frac{kk\alpha}{8k_y k_z L_D}\int_0^{t_D}\frac{e^{-\left[(y_D-y_{wD})^2+(z_D-z_{wD})^2\right]/4\tau}}{\tau}d\tau \tag{4.2}$$

where $\alpha = 2$ for $x_D < 1$, and 0 for $x_D > 1$ for an isotropic reservoir.

4.2 Other flow periods

Early linear, transition or steady-state may occur after the early radial flow. The possibility of linear flow period occurring does not exist if the bottom reservoir boundary is felt first. The bottom layer, which is modeled as a constant-pressure boundary, acts to curb reservoir pressure decline and bring about eventual steady-state. The onset of steady state may be delayed if

(1) $k_h >> k_v$,

(2) production rate is low,

(3) the reservoir thickness is large, and

(4) the well is located near the upper vertical boundary.

If $k_h >> k_v$, flow transients are propagated rapidly along the *x*-axis and this dominates this period until the effects of the ends of the wellbore are felt. But, if the wellbore is sufficiently long in relation to the reservoir thickness and $k_v >> k_h$, the effect of the contiguous bottom water is eventually felt first and steady-state results. However, it should be noted that delaying steady-state in the case considered here is tantamount to prolonging the early radial (infinite-acting, clean oil production) period. Therefore, for an anisotropic reservoir, the dimensionless pressure expression for the second flow period can be written as follows if the lower and upper reservoir boundaries (z-axis) are felt before the ends of the wellbore along the x-axis and the ends of the reservoir along the y-axis:

$$p_D = \frac{kk\alpha}{8L_D k_y k_z}\int_0^{t_D}\frac{e^{-[(y_D-y_{wD})^2+(z_D-z_{wD})^2)]/4\tau}}{\tau}+\frac{\pi}{y_{eD}}\int_{t_{De}}^{t_D}\left[1+2\sum_{m=1}^{\infty}\exp(-\frac{m^2\pi^2\tau}{y_{eD}^2})\cos\frac{mz_D\pi}{y_{eD}}\cos\frac{mz_D\pi}{y_{eD}}\right]\bullet \tag{4.3}$$
$$[erf(\frac{\sqrt{\frac{k}{k_x}}+x_D}{2\sqrt{\tau}})+erf(\frac{\sqrt{\frac{k}{k_x}}-x_D}{2\sqrt{\tau}})]\bullet\sum_{l=1}^{\infty}\exp(-\frac{(2l-1)^2\pi^2\tau}{4h_D^2})\sin\frac{(2l-1)\pi z_{wD}}{2h_D}\sin\frac{(2l-1)\pi z_D}{2h_D}d\tau$$

or,

$$p_D = \frac{kk\alpha}{8k_y k_z L_D}\int_0^{t_D}\frac{e^{-\left[(y_D-y_{wD})^2+(z_D-z_{wD})^2\right]/4\tau}}{\tau}d\tau$$

$$+\frac{2\sqrt{\pi}}{x_{eD}}\sqrt{\frac{k}{k_y}}\int_{t_{De}}^{t_D}\left[1+\frac{2x_{eD}}{\pi}\sum_{n=1}^{\infty}\frac{1}{n}\exp(-\frac{n^2\pi^2\tau}{x_{eD}^2})\sin\frac{n\pi}{x_{eD}}\cos\frac{n\pi x_{wD}}{x_{eD}}\cos\frac{n\pi x_D}{x_{eD}})\right]\bullet \quad (4.4)$$

$$\frac{e^{-y_D-y_{wD})^2/4\tau}}{\sqrt{\tau}}\bullet\sum_{l=1}^{\infty}\exp(-\frac{(2l-1)^2\pi^2\tau}{4h_D^2})\sin\frac{(2l-1)\pi z_{wD}}{2h_D}\sin\frac{(2l-1)\pi z_D}{2h_D}d\tau.$$

if the ends of the reservoir along the *x*-axis and the lower and upper reservoir boundaries are felt first before the ends of the reservoir along the *y*-axis; or,

$$p_D = \frac{kk\alpha}{8k_y k_z L_D}\int_0^{t_D}\frac{e^{-\left[(y_D-y_{wD})^2+(z_D-z_{wD})^2\right]/4\tau}}{\tau}d\tau$$

$$+\frac{\sqrt{\pi}}{4}\sqrt{\frac{k}{k_y}}\int_{t_{De}}^{t_D}[erf\,(\frac{\sqrt{\frac{k}{k_x}}+x_D}{2\sqrt{\tau}})+erf\,(\frac{\sqrt{\frac{k}{k_x}}-x_D}{2\sqrt{\tau}})]\bullet\frac{e^{-y_D-y_{wD})^2/4\tau}}{\sqrt{\tau}}\bullet \quad (4.5)$$

$$\sum_{l=1}^{\infty}\exp(-\frac{(2l-1)^2\pi^2\tau}{4h_D^2})\sin\frac{(2l-1)\pi z_{wD}}{2h_D}\sin\frac{(2l-1)\pi z_D}{2h_D}d\tau$$

if the external boundaries of the reservoir along the z-axis are felt first before the ends of the reservoir along the x-axis and y-axis. However, if the ends of the reservoir boundaries along both y- and z-axes are felt first before the ends of the wellbore, then

$$p_D = \frac{kk\alpha}{8k_y k_z L_D}\int_0^{t_D}\frac{e^{-\left[(y_D-y_{wD})^2+(z_D-z_{wD})^2\right]/4\tau}}{\tau}d\tau +$$

$$\frac{\pi}{y_{eD}}\sqrt{\frac{k}{k_y}}\int_{t_{De}}^{t_D}[erf(\frac{\sqrt{\frac{k}{k_x}}+x_D}{2\sqrt{\tau}})+erf(\frac{\sqrt{\frac{k}{k_x}}-x_D}{2\sqrt{\tau}})]\bullet[1+2\sum_{m=1}^{\infty}\exp(-\frac{m^2\pi^2\tau}{y_{eD}})\cos\frac{m\pi y_{wD}}{y_{eD}}\cos\frac{m\pi y_D}{y_{eD}}]$$

$$\bullet\sum_{l=1}^{\infty}\exp(-\frac{(2l-1)^2\pi^2\tau}{4h_D^2})\sin\frac{(2l-1)\pi z_{wD}}{2h_D}\sin\frac{(2l-1)\pi z_D}{2h_D}d\tau \quad (4.6)$$

Equations (4.1) to (4.6) show that only two general flow periods are observable. These are either

(1) early radial followed by linear periods or

(2) early radial followed by steady-state periods.

If any of the reservoir or wellbore boundaries is not felt before the lower boundary, then such boundary may never be felt again in the course of flow in the wellbore. The emergence of steady-state, as a result of influx and production of water is irreversible. Therefore, the period of clean oil production can be extended by carefully selecting production and wellbore completion options, so that no external boundary is felt. It should be noted that equations (4.1) to (4.5) are intended to show the mandatory early radial period, which flourishes before the effect of any boundary and to assist in the computation of dimensionless pressure gradients throughout any flow period. Another major advantage of this presentation is that gradients so calculated can easily show departures or transitions between flow periods thus helping in the more correct flow period delineation.

Dimensionless pressure gradients of equation (2.2) are uniform for the same flow period, and would change if another kind of flow period or another boundary is encountered. The changes represent fluid flux that is possible due to available swept area. Therefore, the period of oil production may manifest more than one type of dimensionless pressure gradient before the onset of steady-state.

5.0 Computation of dimensionless pressure gradients, p'_D

According to equation (2.2) dimensionless pressure gradients for equations (4.1) to (4.6) are derived, respectively, as

$$\frac{\partial p_D}{\partial t_D}=\frac{kk\alpha e^{-\left[(y_D-y_{wD})^2+(z_D-z_{wD})^2\right]/4t_D}}{8k_y k_z L_D t_D}$$

$$+\frac{4\pi}{x_{eD}y_{eD}}\left[1+\frac{2x_{eD}}{\pi}\sum_{n=1}^{\infty}\frac{1}{n}\exp\left(-\frac{n^2\pi^2 t_D}{x_{eD}^2}\sin\frac{n\pi}{x_{eD}}\cos\frac{n\pi x_{wD}}{x_{eD}}\cos\frac{n\pi x_D}{x_{eD}}\right)\right]\bullet \tag{5.1}$$

$$\left[1+2\sum_{m=1}^{\infty}\exp\left(-\frac{m^2\pi^2 t_D}{y_{eD}^2}\right)\cos\frac{m\pi y_{wD}}{y_{eD}}\cos\frac{m\pi y_D}{y_{eD}}\right)\right]\bullet$$

$$\sum_{l=1}^{\infty}\exp\left(-\frac{(2l-1)^2\pi^2 t_D}{4h_D^2}\right)\sin\frac{(2l-1)\pi z_{wD}}{2h_D}\sin\frac{(2l-1)\pi z_D}{2h_D}$$

$$\frac{\partial p_D}{\partial t_D}=\frac{kk\alpha e^{-\left[(y_D-y_{wD})^2+(z_D-z_{wD})^2\right]/4\tau}}{8k_y k_z L_D t_D} \tag{5.2}$$

$$\frac{\partial p_D}{\partial t_D}=\frac{kk\alpha e^{-\left[(y_D-y_{wD})^2+(z_D-z_{wD})^2\right]/4t_D}}{8k_y k_z L_D t_D}+\frac{\pi}{y_{eD}}\sqrt{\frac{k}{k_y}}\left[erf\left(\frac{\sqrt{\frac{k}{k_x}}+x_D}{2\sqrt{t_D}}\right)+erf\left(\frac{\sqrt{\frac{k}{k_x}}-x_D}{2\sqrt{t_D}}\right)\right].$$

$$\left[1+2\sum_{m=1}^{\infty}\exp\left(-\frac{m^2\pi^2 t_D}{y_{eD}}\right)\cos\frac{m\pi y_{wD}}{y_{eD}}\cos\frac{m\pi y_D}{y_{eD}}\right] \tag{5.3}$$

$$\bullet\sum_{l=1}^{\infty}\exp\left(-\frac{(2l-1)^2\pi^2 t_D}{4h_D^2}\right)\sin\frac{(2l-1)\pi z_{wD}}{2h_D}\sin\frac{(2l-1)\pi z_D}{2h_D}$$

$$\frac{\partial p_D}{\partial t_D}=\frac{kk\alpha e^{-\left[(y_D-y_{wD})^2+(z_D-z_{wD})^2\right]/4t_D}}{8k_y k_z L_D t_D}$$

$$+\frac{2\sqrt{\pi}}{x_{eD}}\sqrt{\frac{k}{k_y}}\left[1+\frac{2x_{eD}}{\pi}\sum_{n=1}^{\infty}\frac{1}{n}\exp\left(-\frac{n^2\pi^2 t_D}{x_{eD}^2}\right)\sin n\frac{\pi}{x_{eD}}\cos n\frac{\pi x_{wD}}{x_{eD}}\cos n\frac{\pi x_D}{x_{eD}}\right]\bullet$$

$$\frac{e^{[(y_D-y\ )^2]/4t_D}}{\sqrt{t_D}}\bullet\sum_{l=1}^{\infty}\exp\left(-\frac{(2l-1)^2\pi^2 t_D}{4h_D^2}\right)\sin\frac{(2l-1)\pi z_{wD}}{2h_D}\sin\frac{(2l-1)\pi z_D}{2h_D} \tag{5.4}$$

$$\frac{\partial p_D}{\partial t_D}=\frac{kk\alpha e^{-\left[(y_D-y_{wD})^2+(z_D-z_{wD})^2\right]/4t_D}}{8k_y k_z L_D t_D}+\frac{\sqrt{\pi}}{2}\sqrt{\frac{k}{k_y}}\left[erf\left(\frac{\sqrt{\frac{k}{k_x}}+x_D}{2\sqrt{t_D}}\right)+erf\left(\frac{\sqrt{\frac{k}{k_x}}-x_D}{2\sqrt{t_D}}\right)\right)\bullet \tag{5.5}$$

$$\frac{e^{[(y_D-y_{wD})^2]/t_D}}{\sqrt{t_D}}\bullet\sum_{l=1}^{\infty}\exp\left(-\frac{(2l-1)^2\pi^2 t_D}{4h_D^2}\right)\sin\frac{(2l-1)\pi z_{wD}}{2h_D}\sin\frac{(2l-1)\pi z_D}{2h_D}$$

Dimensionless wellbore pressure derivatives were computed for a horizontal well parameters: $y_D = y_{wD} = 2 \times 10^{-3}$, $x_D = x_{wD} = 0.732$ (infinite conductivity condition), $z_D = 0.5h_D$, (central well location along the vertical axis), $k_x = k_y = k_z$ (isotropic reservoir case), hence, $h_D = 1/L_D$, different dimensionless well lengths, L_D. Both square and rectangular geometries are considered and are selected through different values of x_{eD} and y_{eD}, $x_{eD} = y_{eD}$ gives a square geometry and otherwise gives a rectangular geometry. However, square and rectangular drainage geometries are considered using only equation (5.1), where all the lateral and vertical boundaries are assumed to have been felt. Equations (5.3) to (5.5) are used to compute dimensionless pressure gradients for cases where at least one external boundary is infinite. Only water arrival pattern into the wellbore is critical to optimization of clean oil production. Elsewhere, that is, in the reservoir, water influx pattern is only critical when sweep and displacement efficiencies are needed. The different geometries considered would help to select suitable well spacing should the size of a field subject to bottom water drive warrant exploitation with one or more horizontal wells. Finally, infinite conductivity well is chosen to determine the propensity of the well to flow unaided (natural flow). Results obtained are shown in Tables 5.1 to 5.4 below.

Table 5.1: Dimensionless pressure derivatives and gradients for rectangular geometry

(a) $(x_{eD}, y_{eD}) = (1,4)$

Dimensionless Time, t_D	$p'_D(t_Dp'_D)$			
	L_D= 0.5	L_D=1.0	L_D=2.5	L_D=10
10^{-5}	50000 (0.5)	25000 (0.25)	10000 (0.1)	2500 (0.025)
10^{-4}	5000 (0.5)	2500 (0.25)	1000 (0.1)	259 (0.0259)
10^{-3}	500 (0.5)	250 (0.25)	108 (0.1)	32 (0.032)
10^{-2}	51.4 (0.514)	30 (0.30)	17 (0.17)	3.3 (0.033)
10^{-1}	6.3 (0.63)	6.1 (0.61)	2.7 (0.27)	0.25 (0.025)
1	1.2 (1.2)	0.61 (0.61)	0.1 (0.1)	0 (0)
10	0.1 (1.0)	0 (0)	0 (0)	0 (0)

(b) $(x_{eD}, y_{eD}) = (1,2)$

Dimensionless Time, t_D	$p'_D(t_Dp'_D)$			
	L_D= 0.5	L_D=1.0	L_D=2.5	L_D=10
10^{-5}	50000(0.5)	25000(0.25)	10000(0.1)	2500(0.025)
10^{-4}	5000(0.5)	2500(0.25)	1000(0.1)	250(0.025)
10^{-3}	500(0.5)	250(0.25)	116(0.116)	40(0.04)
10^{-2}	51(0.51)	34(0.34)	24(0.24)	4.1(0.041)
10^{-1}	6(0.6)	10(1.0)	4.3(0.43)	0.25(0.025)
1	0.83 (0.83)	0.8(0.8)	0.1(0.1)	0(0)
10	0.1(1.0)	0(0)	0(0)	0(0)

(c) $(x_{eD}, y_{eD}) = (2,1)$

Dimensionless Time, t_D	$p'_D(t_Dp'_D)$			
	L_D= 0.5	L_D=1.0	L_D=2.5	L_D=10
10^{-5}	50000(0.5)	25000(0.25)	10000(0.1)	2523(0.02523)
10^{-4}	5000(0.5)	2500(0.25)	1000(0.1)	272(0.0272)
10^{-3}	500(0.5)	261(0.261)	119(0.119)	43(0.043)
10^{-2}	53(0.53)	36(0.36)	26(0.26)	4.5(0.045)
10^{-1}	7.7(0.77)	10(1.0)	4.5(0.45)	0.25(0.025)
1	1.1(1.1)	0.6(0.6)	0.1(0.1)	0(0)
10	0(0)	0(0)	0(0)	0(0)

(d) $(x_{eD}, y_{eD}) = (2,4)$

Dimensionless Time, t_D	$p'_D(t_Dp'_D)$			
	L_D= 0.5	L_D=1.0	L_D=2.5	L_D=10
10^{-5}	50000(0.5)	25000(0.25)	10000(0.1)	2500(0.025)
10^{-4}	5000(0.5)	2500(0.25)	1000(0.1)	256(0.0256)
10^{-3}	501(0.501)	253(0.253)	105(0.105)	30(0.030)
10^{-2}	51(0.51)	28(0.28)	14.2(0.142)	3.0(0.030)
10^{-1}	5.6(0.56)	4.7(0.47)	2.0(0.20)	0.25(0.025
1	0.56(0.56)	0.45(0.45)	0.1(0.1)	0(0)
10	0(0)	0(0)	0(0)	0(0)

(e) $(x_{eD}, y_{eD}) = (4,2)$

Dimensionless Time, t_D	$p'_D(t_Dp'_D)$			
	L_D= 0.5	L_D=1.0	L_D=2.5	L_D=10
10^{-5}	50000(0.5)	25000(0.25)	10000(0.1)	2500(0.025)
10^{-4}	5000(0.5)	2500(0.25)	1000(0.1)	260(0.026)
10^{-3}	511(0.511)	255(0.255)	109(0.109)	33(0.033)
10^{-2}	61(0.61)	30(0.30)	17.8(0.178)	6.0(0.06)
10^{-1}	15(1.5)	6.5(0.65)	3.0(0.3)	0.25(0.025)
1	4.1(4.1)	0.57(0.57)	0.1(0.1)	0(0)
10	0.1(1.0)	0(0)	0(0)	0(0)

Table 5.2: Dimensionless pressure derivatives and gradients for square geometry

(a) $(x_{eD}, y_{eD}) = (1,1)$

Dimensionless Time, t_D	$p'_D(t_Dp'_D)$			
	L_D= 0.5	L_D=1.0	L_D=2.5	L_D=10
10^{-5}	50000(0.5)	25000(0.25)	10000(0.1)	2538(0.02538)
10^{-4}	5000(0.5)	2500(0.25)	1000(0.1)	286.8(0.02868)
10^{-3}	505.5(0.5)	268.8(0.2688)	131(0.131)	54.4(0.0544)
10^{-2}	55.4(0.554)	43(0.43)	37(0.37)	8.1(0.081)
10^{-1}	9.4(0.94)	14.6(1.46)	6.9(0.69)	0.25(0.025)
1	1.7(1.7)	0.9(0.9)	0.1(0.1)	0(0)
10	0.1(1.0)	0(0)	0(0)	0(0)

(b) $(x_{eD}, y_{eD}) = (2,2)$

Dimensionless Time, t_D	$p'_D(t_Dp'_D)$			
	L_D= 0.5	L_D=1.0	L_D=2.5	L_D=10
10^{-5}	50000(0.5)	25000(0.25)	10000(0.1)	2500(0.025)
10^{-4}	5000(0.5)	2500(0.25)	1000(0.1)	261(0.0261)
10^{-3}	500(0.5)	256(0.256)	110(0.110)	34(0.034)
10^{-2}	51.7(0.517)	30.5(0.305)	18.3(0.183)	3.5(0.035)
10^{-1}	6.5(0.65)	6.7(0.67)	3.0(0.30)	0.3(0.03)
1	1.0(1.0)	0.6(0.6)	0.1(0.1)	0(0)
10	0.1(1.0)	0(0)	0(0)	0(0)

Table 5.3: Dimensionless pressure derivatives and gradients when x_{eD} is not felt and y_{eD} boundaries are sealed

(a) (x_{eD}, y_{eD})= (1,4)

Dimensionless Time, t_D	$p'_D(t_Dp'_D)$			
	L_D= 0.5	L_D=1.0	L_D=2.5	L_D=10
10^{-5}	50000(0.5)	25000(0.25)	10000(0.1)	2500(0.025)
10^{-4}	5000(0.5)	2500(0.25)	1000(0.1)	251(0.0251)
10^{-3}	500(0.5)	250(0.25)	100(0.1)	25(0.025)
10^{-2}	50(0.5)	25(0.25)	10.5(0.105)	2.5(0.025)
10^{-1}	5.5(0.55)	2.7(0.27)	1.0(0.1)	0.3(0.03)
1	0.62(0.62)	0.3(0.30)	0.1(0.1)	0(0)
10	0.1(1.0)	0(0)	0(0)	0(0)

(b) $(x_{eD}, y_{eD}) = (1,2)$

Dimensionless Time, t_D	$p'_D(t_Dp'_D)$			
	L_D= 0.5	L_D=1.0	L_D=2.5	L_D=10
10^{-5}	50000(0.5)	25000(0.25)	10000(0.1)	2500(0.025)
10^{-4}	5000(0.5)	2500(0.25)	1000(0.1)	251(0.0251)
10^{-3}	500(0.5)	250(0.25)	100(0.1)	25(0.025)

10^{-2}	50(0.5)	25.4(0.254)	10(0.1)	2.5(0.025)
10^{-1}	6.0(0.6)	2.6(0.26)	1(0.1)	0.3(0.03.)
1	0.7(0.7)	0.3(0.3)	0.1(0.1)	0(0)
10	0.1(1.0)	0(0)	0(0)	0(0)

(c) $(x_{eD}, y_{eD}) = (2,1)$

Dimensionless Time, t_D	$p'_D(t_Dp'_D)$			
	L_D= 0.5	**L_D=1.0**	**L_D=2.5**	**L_D=10**
10^{-5}	50000(0.5)	25000(0.25)	10000(0.1)	2500(0.025)
10^{-4}	5000(0.5)	2500(0.25)	1000(0.1)	250(0.025)
10^{-3}	502(0.502)	250(0.25)	100(0.1)	25(0.025)
10^{-2}	52.1(0.521)	25(0.25)	10(0.1)	2.5(0.025)
10^{-1}	6.1(0.61)	2.6(0.26)	1.0(0.1)	0.3(0.03)
1	0.8(0.8)	0.3(0.3)	0.1(0.1)	0(0)
10	0.1(1.0)	0(0)	0(0)	0(0)

Table 5.4: Dimensionless pressure Derivatives and Gradients when y_{eD} is not felt and x_{eD} boundaries are sealed

(a) $(x_{eD}, y_{eD}) = (1,4)$

Dimensionless Time, t_D	$p'_D(t_Dp'_D)$			
	L_D= 0.5	**L_D=1.0**	**L_D=2.5**	**L_D=10**
10^{-5}	50164(0.5)	25560(0.26)	10953(0.11)	3618(0.036)
10^{-4}	5052(0.5)	2677(0.27)	1301(0.13)	596(0.060)
10^{-3}	516(0.52)	306(0.31)	194(0.19)	112(0.11)
10^{-2}	55(0.55)	42(0.42)	36(0.36)	5.5(0.055)
10^{-1}	6.5(0.65)	3.1(0.31)	3.0(0.30)	0.3(0.03)
1	0.8(0.8)	0.9(0.9)	0.1(0.1)	0(0)
10	0.2(2.0)	0.2(2.0)	0(0)	0(0)

(b) $(x_{eD}, y_{eD}) = (2,1)$

Dimensionless Time, t_D	$p'_D(t_Dp'_D)$			
	L_D= 0.5	**L_D=1.0**	**L_D=2.5**	**L_D=10**
10^{-5}	50099(0.5)	25339(0.25)	10576(0.1)	3176(0.032)
10^{-4}	5031(0.5)	2607(0.26)	1182(0.12)	459(0.046)
10^{-3}	510(0.51)	284(0.284)	157(0.16)	78(0.078)
10^{-2}	53(0.53)	35.4(0.354)	26(0.26)	4.5(0.045)
10^{-1}	6.0(0.6)	5.0(0.5)	2.0(0.20)	0.30(0.03)
1	0.6(0.6)	0.40(0.40)	0.1(0.1)	0(0)
10	0.1(1.0)	0(0)	0(0)	0(0)

(c) $(x_{eD}, y_{eD}) = (4,2)$

Dimensionless Time, t_D	$p'_D(t_Dp'_D)$			
	L_D= 0.5	**L_D=1.0**	**L_D=2.5**	**L_D=10**
10^{-5}	50093(0.5)	2819(0.28)	10543(0.1)	3137(0.031)
10^{-4}	5029(0.50)	361(0.36)	1171(0.12)	447(0.045)
10^{-3}	509(0.51)	57(0.57)	154(0.15)	75(0.075)
10^{-2}	53(0.53)	12.3(0.12)	25(0.25)	4.2(0.042)
10^{-1}	6.0(0.6)	2.7(0.27)	2.7(0.27)	0.3(0.03)
1	0.9(0.9)	0.1(0.1)	5.5(5.5)	0(0)
10	0.1(1.0)	0(0)	0.4(4.0)	0(0)

6.0 Results and discussion

6.1 Early Time

$p'_D \approx 1/(4\, t_D\, L_D)$ for cases represented by equations (5.1) and (5.3) L_D and t_D govern dimensionless gradients. But in equations (5.5) and (5.4), at $t_D \geq 10^{-6}$, the reservoir geometry and well length affect flow gradients.

6.2 Late Time

First and final steady-state is attained faster the larger the L_D. Larger L_D yield lower p'_D. However, some maximum points are observed across the ranges of dimensionless lengths chosen. For an isotropic reservoir case x_{eD} = 2.0 means full well penetration of the reservoir along the x-axis, but for values of x_{eD} > 2.0, there is partial penetration. Partial penetration gives rise to limited reservoir exposure to fluid flow. This accounts for the larger dimensionless pressure gradients observed for all cases of x_{eD} > 2.0 for the same L_D.

For all the cases of reservoir geometries considered, dimensionless flow gradients decrease with increasing dimensionless well length. When all the reservoir boundaries are felt (late time flow), dimensionless wellbore pressure gradients are inversely proportional to the product of lateral extents; i.e., ($x_{eD}y_{eD}$) for the same L_D. This means that for the same t_D , small reservoirs produce the effects of larger dimensionless pressure drop than larger reservoirs. The implication of this is that, given the same sensitivity of an aquifer body and well completion, small reservoirs would experience earlier water production than large reservoir. The effects of early water production by small reservoirs may be mitigated by well length extension. Meanwhile, geometries of the same dimensionless area but different widths, e.g. (x_{eD} ,y_{eD}) = (1,4) and (x_{eD} ,y_{eD}) = (2,2), have different dimensionless pressure gradients when their extremities are eventually felt at late flow dimensionless times. This behaviour shows that the effect of square reservoir geometry can be produced by a rectangular geometry, and vice versa, by simply modifying the wellbore length (either by further drilling, stimulation or plug back). This is the only option available to an operator because the reservoir area cannot be modified. This guideline can be used to select drainage areas, and therefore well spacing, in a field containing a network of horizontal wells, all subject to bottom water drive energy.

Results in Table 5.4 and Table 5.3, show that for the same reservoir geometry, larger dimensionless pressure gradients are obtained if the x_{eD} boundaries are felt first than the y_{eD} boundaries before steady-state effects. If the y_{eD} boundaries are felt first, gradients are actually the same for early times ($t_D \leq 10^{-6}$) for all L_D as for most geometries. But, if the x_{eD} boundaries are felt first, the gradients are larger for the $t_D \leq 10^{-6}$ for all L_D. However, if the reservoir is sufficiently large such that none of the lateral extremities is felt during the period of clean oil production, results in Table 5.4 show that sufficiently high gradients, comparable to those in Figure 6.1 are obtained. These results clearly show that, if the reservoir experiences infinitely far away lateral boundaries, it has tremendously high propensity to produce clean oil.

7.0 Computation of dimensionless pressure derivative, $t_D p'_D$

Dimensionless pressure derivative expressions for equations (4.1) to (5.5), derived according to equation (2.3) are

$$t_D \frac{\partial p_D}{\partial t_D} = \frac{kk\alpha e^{-\left[(y_D - y_{wD})^2 + (z_D - z_{wD})^2\right]/4t_D}}{8k_y k_z L_D} \tag{7.1}$$

$$t_D \frac{\partial p_D}{\partial t_D} = \frac{kk\alpha e^{-\left[(y_D - y_{wD})^2 + (z_D - z_{wD})^2\right]/4t_D}}{8k_y k_z L_D} + \frac{\pi t_D}{y_{eD}}\sqrt{\frac{k}{k_y}}.[erf(\frac{\sqrt{\frac{k}{k_x}} + x_D}{2\sqrt{t_D}}) + erf(\frac{\sqrt{\frac{k}{k_x}} - x_D}{2\sqrt{t_D}})]$$

$$[1 + 2\sum_{m=1}^{\infty}\exp(-\frac{m^2\pi^2 t_D}{y_{eD}})\cos\frac{m\pi y_{wD}}{y_{eD}}\cos\frac{m\pi y_D}{y_{eD}}] \tag{7.2}$$

$$\bullet \sum_{l=1}^{\infty}\exp(-\frac{(2l-1)^2\pi^2 t_D}{4h_D^2})\sin\frac{(2l-1)\pi z_{wD}}{2h_D}\sin\frac{(2l-1)\pi z_D}{2h_D}$$

$$t_D \frac{\partial p_D}{\partial t_D} = \frac{kk\alpha e^{-\left[(y_D-y_{wD})^2+(z_D-z_{wD})^2\right]/4t_D}}{8k_y k_z L_D} + \frac{\sqrt{\pi}t_D}{2}\sqrt{\frac{k}{k_y}}[erf(\frac{\sqrt{\frac{k}{k_x}}+x_D}{2\sqrt{t_D}})+erf(\frac{\sqrt{\frac{k}{k_x}}-x_D}{2\sqrt{t_D}})]\bullet \tag{7.3}$$

$$\frac{e^{[(y_D-y_{wD})^2]/t_D}}{\sqrt{t_D}} \bullet \sum_{l=1}^{\infty}\exp(-\frac{(2l-1)^2\pi^2 t_D}{4h_D^2})\sin\frac{(2l-1)\pi z_{wD}}{2h_D}\sin\frac{(2l-1)\pi z_D}{2h_D}$$

$$t_D \frac{\partial p_D}{\partial t_D} = \frac{kk\alpha e^{-\left[(y_D-y_{wD})^2+(z_D-z_{wD})^2\right]/4t_D}}{8k_y k_z L_D}$$

$$+\frac{2t_D\sqrt{\pi}}{x_{eD}}\sqrt{\frac{k}{k_y}}[1+\frac{2x_{eD}}{\pi}\sum_{n=1}^{\infty}\frac{1}{n}\exp(-\frac{n^2\pi^2 t_D}{x_{eD}^2})\sin n\frac{\pi}{x_{eD}}\cos n\frac{\pi x_{wD}}{x_{eD}}\cos n\frac{\pi x_D}{x_{eD}}]\bullet \tag{7.4}$$

$$\frac{e^{[(y_D-y_{wD})^2]}}{\sqrt{t_D}} \bullet \sum_{l=1}^{\infty}\exp(-\frac{(2l-1)^2\pi^2 t_D}{4h_D^2})\sin\frac{(2l-1)\pi z_{wD}}{2h_D}\sin\frac{(2l-1)\pi z_D}{2h_D}$$

$$t_D \frac{\partial p_D}{\partial t_D} = \frac{kk\alpha e^{-\left[(y_D-y_{wD})^2+(z_D-z_{wD})^2\right]/4t_D}}{8k_y k_z L_D}$$

$$+\frac{4\pi t_D}{x_{eD}y_{eD}}\left[1+\frac{2x_{eD}}{\pi}\sum_{n=1}^{\infty}\frac{1}{n}\exp(-\frac{n^2\pi^2 t_D}{x_{eD}^2}\sin\frac{n\pi}{x_{eD}}\cos\frac{n\pi x_{wD}}{x_{eD}}\cos\frac{n\pi x_D}{x_{eD}})\right] \tag{7.5}$$

$$\bullet\left[1+2\sum_{m=1}^{\infty}\exp(-\frac{m^2\pi^2 t_D}{y_{eD}^2})\cos\frac{m\pi y_{wD}}{y_{eD}}\cos\frac{m\pi y_D}{y_{eD}})\right]$$

$$\bullet\sum_{l=1}^{\infty}\exp(-\frac{(2l-1)^2\pi^2 t_D}{4h_D^2})\sin\frac{(2l-1)\pi z_{wD}}{2h_D}\sin\frac{(2l-1)\pi z_D}{2h_D}.$$

The same parameters used for computing gradients were used to compute all the values of $t_D\partial p_D/\partial t_D$. The results are shown in Tables 5.1 to 5.4. At early times, dimensionless pressure derivatives are governed chiefly by dimensionless well length, and is approximately given as $1/(4L_D)$ for an anisotropic reservoir. In all the cases considered, single maximum points were observed at t_D approximately equal to $1/L_D$ and independent of reservoir geometry. For $L_D = 2.5$, however, there is sudden collapse of derivative immediately after $t_D = 1/(4L_D)$ for some reservoir geometries. For all cases, onset of steady-state is characterized by rise in dimensionless pressure derivative for $t_D > 1/(4L_D)$. These dimensionless times would correspond to the last change in $\partial p_D/\partial t_D$ plot since the encroaching water is incompressible.

At late dimensionless times only, when the lateral boundaries are felt, square reservoirs yield dimensionless pressure derivatives that are inversely proportional to the product x_{eD} y_{eD}. But, during the same dimensionless times derivatives for rectangular geometries behave differently. In this case, increases in y_{eD} produce decreasing derivatives for fixed x_{eD} and L_D. Furthermore, increases in x_{eD} for fixed y_{eD} and L_D either produce increasing or decreasing dimensionless pressure derivatives depending on well penetration along the x-axis. For fully penetrating wells, lower values of derivatives are obtained for late dimensionless times, while larger values are obtained for cases of partial penetration. The same behaviour was observed for dimensionless pressure gradients.

When no lateral boundary is felt, pressure gradients are as high as when either or both lateral boundaries is/are felt. This mean that the best well completion, which could also give high productivity, is achieved if no lateral reservoir boundary is felt during flow. Such completion could be stimulated for further clean oil production if well penetration, especially along the x-axis is implemented. The dimensionless pressure derivatives, on the other hand, show in Figure 7.1 that, if both x_{eD} and y_{eD} boundaries are not felt, that is, still infinitely far, derivatives are greater than those obtained if the y_{eD} values are felt and x_{eD} infinite by the quantity:

$$\frac{2t_D\sqrt{\pi}}{x_{eD}}\sqrt{\frac{k}{k_y}}[1+\frac{2x_{eD}}{\pi}\sum_{n=1}^{\infty}\frac{1}{n}\exp(-\frac{n^2\pi t_D}{x_{eD}^2})\sin\frac{n\pi}{x_{eD}^2}\cos\frac{n\pi x_D}{x_{eD}}\cos\frac{n\pi x_{wD}}{x_{eD}}] \qquad (7.6)$$

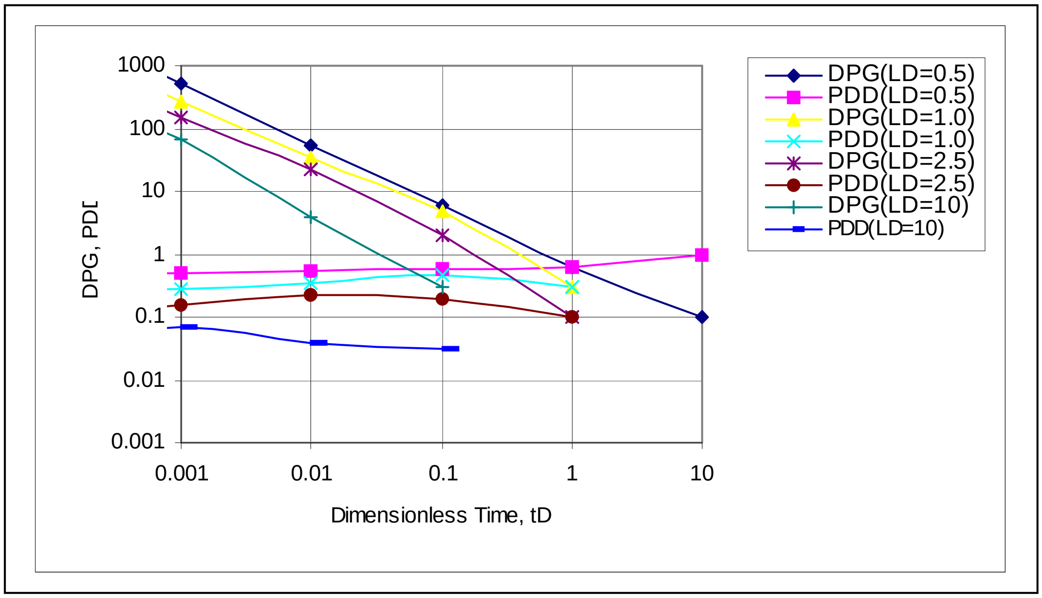

Figure 7.1: Derivatives for reservoir flow unaffected by external extents

for all dimensionless flow times and reservoir geometries. However, those completions with all infinite lateral boundaries are lower by the quantity:

$$\frac{t_D\sqrt{\pi}}{x_{eD}}\sqrt{\frac{k}{k_y}}[1+\frac{2x_{eD}}{\pi}\sum_{n=1}^{\infty}\frac{1}{n}\exp(-\frac{n^2\pi t_D}{x_{eD}^2})\sin\frac{n\pi}{x_{eD}^2}\cos\frac{n\pi x_D}{x_{eD}}\cos\frac{n\pi x_{wD}}{x_{eD}}]\bullet\frac{e^{-(y_D-y_{wD})^2/4t_D}}{\sqrt{t_D}} \qquad (7.7)$$

for all dimensionless times and for all reservoir geometries; that is, about half of equation (7.7)

8.0 Conclusion

Well completion type is very crucial to ultimate oil recovery from any given reservoir system, even with a horizontal well. Water influx or eventual production from any kind of well completion is inimical to the economics of oil and gas production. Pressure derivatives and gradients are capable of exposing the true character of an entire reservoir system. At any stage in the life of a well, these characteristics can be used to decide on the best production method that can guarantee more economic production. To adequately take advantage of the characteristics presented by a reservoir system, a basic understanding is imperative. This is the major reason why this study is necessary for a horizontal well under the influence of bottom water.

In this paper, pressure derivatives and gradients of a bottom water drive reservoir drained with a horizontal were calculated and factors affecting clean oil production were investigated. The following major conclusions were drawn from this study:

(1) p'_D and $t_D\, p'_D$ are both inversely proportional to L_D and the product ($x_{eD}y_{eD}$), at early and late flow times, respectively.

(2) Large reservoirs have the tendency to produce clean oil longer than small reservoirs of the same well completion and reservoir properties.

(3) Both p'_D and $t_D\, p'_D$ exhibit single maximum points on log-log plots against t_D at $t_D = 1/(4L_D)$.

(4) At water breakthrough, $t_D\, p'_D$ collapses to zero; water fillup (onset of steady state) follows the maximum point.

(5) Well length modification can produce the effects of a square reservoir for a rectangular reservoir and vice versa.
(6) Depending on flow rate, reservoir anisotropy, aquifer responsiveness, more than two flow periods may be achievable for a particular well completion.

References

[1] Bourdet,D., Whittle,T.M., Douglas, A.A., and Pirard, Y-M.: "A New Set of Type Curves Simplifies Well Test Analysis," World Oil, (May 1983), 95 – 106.

[2] Bourdet, D., Ayoub, J.A., and Pirard, Y-M.: "Use of the Pressure Derivative in Well Test Interpretation," SPE Formation Evaluation, (June 1989), 293 – 302.

[3] Ozkan, E. and Raghavan, R.: "Performance of Horizontal Wells Subject to Bottom Water Drive," *SPERE* (Aug. 1990) 375-383.

[4] Onur, M., Yeh, N.S. and Reynolds, A.C.: "New Applications of the Pressure Derivative in Well Test Analysis," SPE Formation Evaluation, (Sept. 1989), 429 – 437.

[5] Tiab, D. and Kumar, A.: "Application of the p_D' Function to Interference Analysis," J.P.T. (Aug. 1980), 1465 – 70.

[6] Malekzadeh, D. and Tiab, D.: "Interference Testing of Horizontal Wells," paper SPE 22793 Presented at the Annual Technical Conference and Exhibition of SPE held in Dallas, TX. Oct. 6-9, 1991.

[7] Gringarten, A.C. and Ramey, H.J.Jr.: "The Use of Source and Green's Functions in Solving Unsteady Flow Problems in Reservoirs," SPE *Trans*., AIME, 1973, 225-285.

[8] Carslaw, H.S. and Jaeger, J.C. : Conduction of Heat through Solids, 2nd Ed. ,Oxford U. Press, London, England (1959).